# Spontaneous Correlation of Crystallographic Orientations in Crystallite Aggregation: Physical Origin and Its Influence on Pattern Formation

**Da-Wei Li,[†] Mu Wang,*[,†] Peng Liu,[‡] Ru-Wen Peng,[†] and Nai-Ben Ming[†]**

*National Laboratory of Solid State Microstructures and Department of Physics, Nanjing University, Nanjing 210093, China, and Beijing Synchrotron Radiation Facility (BSRF), Institute of High Energy Physics, Chinese Academy of Sciences, Beijing 100039, China*

*Received: July 26, 2002; In Final Form: October 9, 2002*

In our previous work we demonstrated an unusual crystallite aggregate in which the crystallites correlate in crystallographic orientation and form a fractal pattern with strong anisotropy (Wang, M.; et al. *Phys. Rev. Lett*. **1998,** *80*, 3089. Liu, X. Y.; et al. *J. Cryst. Growth* **2000,** *208*, 687.). Yet it remains unanswered why each crystallite appears with specific orientation and obeys a strict order. Here we report an in-depth study of the origin of the long-range correlation of the crystallographic orientations in the aggregate investigated by means of micro-X-ray-diffraction, atomic force microscopy, and in-situ optical observation. The experimental data suggest that the topographic regularity of the aggregate arises from the consecutive rotation of the crystallographic orientation in the nucleation-mediated growth. This effect may occur when nucleation takes place in a region with inhomogeneous surface tension, and may help us to understand the long-range ordering effect in aggregating crystallites.

## I. Introduction

Self-organization of microstructures in the interfacial growth has been intensively studied in the past decades.[1−7] Ordered structures can be spontaneously generated in the interfacial growth by stress-induced instability. When a crystalline layer is coherently adsorbed on a substrate with different lattice parameters, the mismatch energy is high and the system tends to escape to a state with lower energy. Instead of generating defects, such as misfit dislocations,[6] the strained film can be relaxed by surface deformation,[1,6] where periodic hills and valleys are induced on the surface. In some cases the film may even split into separated clusters.[8] This stress release mechanism was first predicted by Asaro and Tiller,[9] and systematically studied by Grinfield.[10] Up to now, most studies of the stress-induced instability concentrate on two-dimensional systems, such as thin films. The stress-induced instability should occur in other systems as well. In crystallization, spontaneous alignment of crystallites and hence ordered aggregation of crystallites have been observed, yet the mechanism remains unclear. One example is the spherulite growth, in which crystallites are continuously twisted or titled. Spherulite growth appears very often in the solidification of polymers[11−13] and certain inorganic materials.[14−16] Another example is the aggregation of $NH_4Cl$ crystallites in agarose gel, where the orientation of each crystallite is closely correlated. Ultimately the branches with regular zigzagged microscopic features are formed.[17,18] Strom et al.[19] point out that two types of zigzagged branches with different crystallite orientations exist. In one case the octahedron {111} is the primary face, whereas in the other case, the hexahedron {100} dominates. The hexahedron {100} and octahedron {111} have comparable energy, so they have equal probability of occurrence. Moreover, the aggregate with spatial periodic roughening transition on the surface has been observed,[20] and such a transition can be attributed to the regular change of crystallographic orientation of the crystallites. It is therefore interesting to find out how these regular structures develop and why they are generated.

In this article we discuss the origin of the long-range correlation of the crystallographic orientations in aggregating crystallite on bases of the data of micro-X-ray-diffraction, atomic force microscopy and in situ optical microscopy. By analyzing these data, we suggest that the regularity of the topography of the aggregate originate from the consecutive rotation of the crystallographic orientation in a nucleation-mediated layered growth. This effect has never been reported before and could be helpful to understand the long-range ordering effect in many cases of crystallization.

## II. Experimental Method

The experiments were carried out in a thin layer of agarose gel containing $NH_4Cl$, sandwiched between two carefully cleaned glass plates. The separation of the glass plates was kept 100 $\mu$m for all runs. The gel was prepared by dissolving agarose (Merck) into ultrapure water (resistivity 18.7 M$\Omega$·cm). The concentration of agarose was 0.25 wt %. $NH_4Cl$ was added into the agarose solution, and the concentration of $NH_4Cl$ was kept at 4.0 wt %. The solution was filled into the space between the two glass plates. The compact gel was formed by cooling. The growth cell was then placed in a chamber with dry environment. Supersaturation, the driving force for crystallization, was generated by evaporating water in the agarose gel through the edges of the glass plates. In this experiment water evaporation was not accurately controlled. Nevertheless, it was a slow process, especially when a shell of $NH_4Cl$ and agarose gel was formed along the edge of the glass plates.[17,18,20] Since the typical

* To whom correspondence should be addressed. E-mail: muwang@netra.nju.edu.cn.

[†] National Laboratory of Solid State Microstructures and Department of Physics.

[‡] Beijing Synchrotron Radiation Facility (BSRF).

10.1021/jp026615v CCC: $25.00 
Published on Web 11/27/2002

duration for in situ optical observation was usually between 10 and 30 min, which was much shorter comparing with the whole evaporation process (typically 15 to 30 h), the driving force for crystallization can be regarded as a constant during the time of observation. The aggregation process was observed in situ by an optical microscope (Orthoplan-pol, Leitz, Germany) with a charge-coupled device (CCD) video system. The aggregate was further analyzed ex situ by means of micro-X-ray-diffraction with the white light from synchrotron radiation (BSRF, Beijing, China), and with an atomic force microscope (Nanoscope IIIa, Digital Instruments, Santa Barbara, CA).

### III. Results and Discussion

The aggregate branch may consist of crystallites with either hexahedron {100} or octahedron {111} as dominant faces. Here we focus on the case in which hexahedron {100} dominant. The aggregate of $NH_4Cl$ crystallites is illustrated in Figure 1a, which is fractal-like. Despite the ramified feature on a large scale, microscopically each branch possesses a deterministic zigzagged feature (Figure 1b). It seems that the diffusion field decides which branch will grow forward and which one will stay behind (screening effect). The average growth rate of the aggregate depends on the supersaturation. For the pattern shown in Figure 1a, the typical growth rate is of the order of 2 $\mu$m/s. The diffusion coefficient in the gel system is of the order of $1 \times 10^{-6}$ cm$^2$/s. It follows that the thickness of the concentration boundary layer, which is the characteristic length of the diffusion field, is of the order of 50 $\mu$m. Indeed we can find in Figure 1a,b that no regularity can be identified among the branches above the scale of about 50 microns. We expect that beyond this length scale the diffusive instability controls the branch morphology and is responsible for the formation of the ramified fractal-like patterns.

Figure 1c shows the detailed morphology of the zigzagged branch observed with AFM. Two types of crystallites can be identified. One is pyramid-like, and is marked by $A_i$ ($i$ = 1, 2, 3, and 4). The crystallites $A_i$ are connected by the other type of crystallites, $B_i$ ($i$ = 1, 2, and 3), which are elongated. The alternating appearance of the crystallites $A_i$ and $B_i$ eventually generates the regularly zigzagged branches shown in Figure 1b. The development of aggregate branch observed with an optical microscope is illustrated in Figure 2. As that will be shown later, the crystallite size depends on the driving force of crystallization. To obtain a sufficiently large crystallite for clear optical observation, we carried out the experiment with lower supersaturation. As illustrated in Figure 2a,b, one of the corners of an *A*-type crystallite grows faster and becomes cusp. Selection of the specific corner is decided by the local concentration field. As the tip of the branch grows further, gradually it broadens and develops into the crystallite $A'$, which is a mirror image of *A* (Figure 2e−g). The previous cusp of *A* turns into an elongated crystallite (type *B*). As demonstrated in Figure 2d−f, one of the corners of $A'$ grows faster and is sharpened. A new cusp is generated eventually, and evolves into a new *B*-type crystallite. In the meantime the direction of branch growth deviates for about 60°. By repeating this process a zigzagged branch is formed. Figure 2e−h shows that the lower right part of the crystallite $A'$ grows much slower than its upper left part. Consequently, the corner in the upper left part of $A'$ sharpens much faster. The difference in the growth rate of the same crystallite along two equivalent crystallographic directions may be due to the inhomogeneous distribution of the concentration field around the crystallite. The nutrient transfer to the lower right part of $A'$ is screened by the neighboring branches.

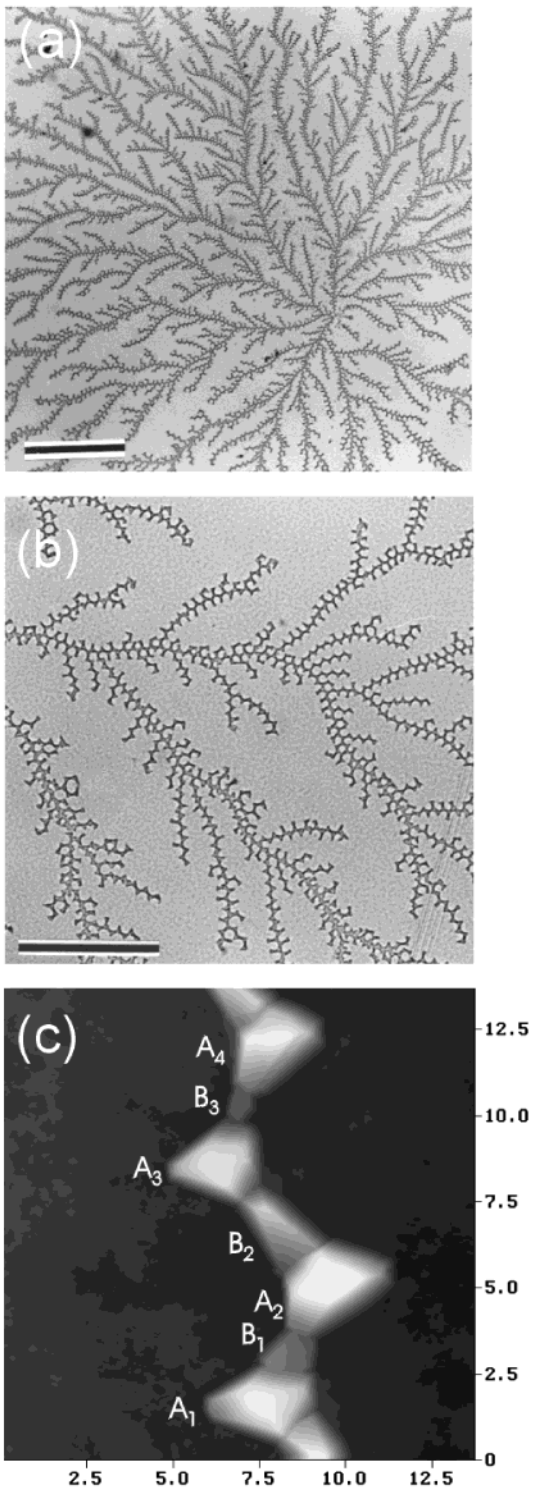


**Figure 1.** (a) The optical micrograph of the crystallite aggregate of $NH_4Cl$. On a large scale the aggregate is random and ramified. The bar represents 100 $\mu$m. (b) Each branch in the fractal-like aggregate consists of a regularly zigzagged structure. The bar represents 50 $\mu$m. (c) The AFM micrograph of the zigzagged branch, in which two types of crystallites $A_i$ and $B_i$ ($i$ = 1, 2, 3, ...) can be identified. These two type of crystallites appear alternatively.

It is interesting to note that the crystallites in the zigzagged branch actually originate from the same ancestor. As indicated by the dark arrows in Figure 2d−g, when the crystallite $A'$ becomes sufficiently large, a ditch appears and finally separates the crystallite $A'$ with crystallite *B*. The similar process takes place in the elongation of the upper left part of the crystallite

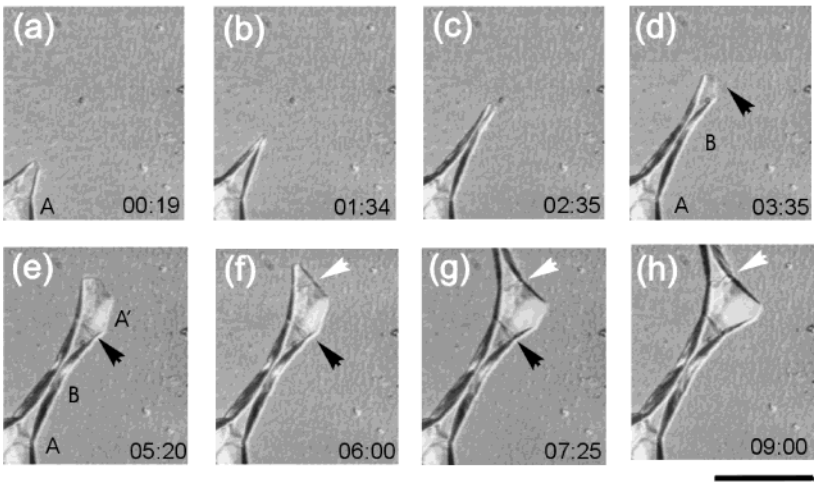


**Figure 2.** The optical micrographs illustrating the growing process of the zigzagged branch. The bar stands for 100 $\mu$m. The digits on each frame stand for minutes and seconds, respectively.

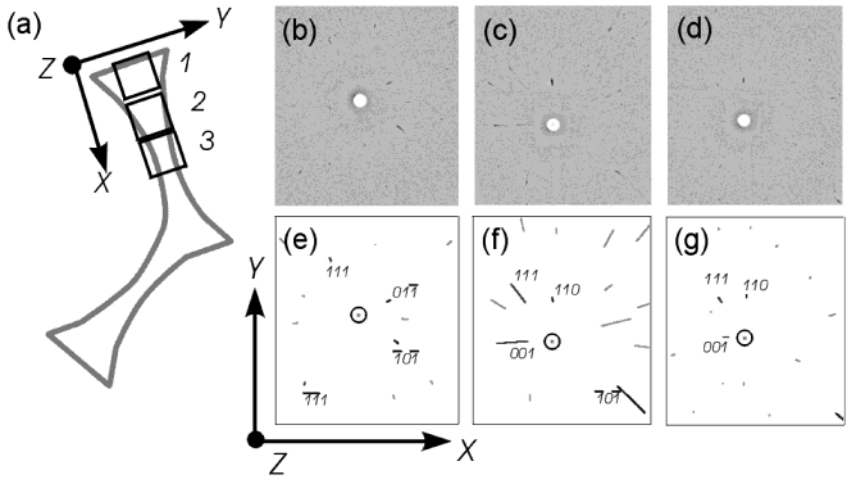


**Figure 3.** The microstructure of the zigzag branch studied by micro-diffraction with white light X-ray from synchrotron radiation. (a) Schematic showing the three sites where micro-diffractions have been carried out. (b−d) The Laue diffraction pattern at sites 1−3, respectively. (e−g) Illustration of the computer simulated diffraction patterns. One may easily find the correspondence between experimental measurements (b−d) and computer simulations (e−g). Comparing the diffraction spots in (c) and (d) (or (f) and (g)), one may easily find that the deviation of the crystallographic orientation at site 2 and site 3 is much smaller than that at site 1 and site 2, suggesting that site 2 and site 3 may locate on the same piece of crystallite (type *B* in Figure 1c).

*A′*, as marked by the white arrows in Figure 2f−h. In other words, repeated processes of corner sharpening and crystallite breaking as the branch extends exist.

To find out why the aggregation follows such regularity, and how the crystallographic orientation evolves during crystallization, we carried out micro-X-ray-diffraction (MXRD) with the white light from the synchrotron radiation. The light spot was $20 \times 20$ $\mu$m$^2$ in size, and an optical microscope helped to direct the beam to the exact sites where we intended to investigate. A sensitive, high-resolution image plate recording system (Fujitsu BASS2500) was used to record the diffraction pattern. Both the image plate and the glass substrate with crystallite aggregate on it were perpendicular to the X-ray beam. The image plate was placed 130 mm behind the sample, so it recorded the small angle diffraction of the crystallites. Figure 3a schematically shows the sites on the zigzagged branch where the experiments of MXRD were carried out. Figure 3b−d shows the experimentally recorded diffraction pattern at sites 1, 2, and 3, respectively. It can be seen that many diffraction spots are elongated. It should be pointed out that the thickness of the crystallite in the aggregate is about 3 $\mu$m, and the width is about 15 $\mu$m in average, which are determined by atomic force microscopy and optical microscopy. According to the Scherrer formula,[21] the angular width of the diffraction spots can be expressed as

$$\beta = \frac{K\lambda}{T\cos\theta} \tag{1}$$

where $K$ is the Scherrer factor, a constant related to the crystallite size and the shape. In most cases $K$ can be taken as 1. $T$ is the thickness of the crystallite; $\lambda$ is the wavelength of the X-ray and $\theta$ is the diffraction angle determined by Bragg equation. For the small angle diffraction cos $\theta$ equals approximately to 1. It follows that the angular width of the diffraction spots will be of the order of 0.04 mRod. By taking the separation of the sample and the image plate (130 mm) into account, immediately we get the spread of the diffraction spots as 5 $\mu$m. Whereas the elongation of the diffraction spots shown in Figure 3b−d is of the order of several millimeters, which is about 3 orders of magnitude larger than that induced by the size effect. Therefore, we conclude that the elongation of diffraction spots is unlikely to be related to crystallite size. Instead, it implies that each crystallite is no longer monocrystalline, i.e., the crystallographic

orientation changes continuously for a few degrees within each crystallite. In other words, the crystallite has been bent along a certain direction. As that will be shown later, it has been observed that the crystallite develops with the mode of layer-by-layer growth. Suppose each layer changes its orientation slightly with respect to the neighboring one, we compile a computer program to simulate the pattern of Laue diffraction. In the simulation we only consider the kinematical diffraction of X-ray. The distribution of the wavelength of X-ray and the crystallographic data of $NH_4Cl$ crystal are known. We let the computer change the initial crystallite orientation and the axis of slice rotation, and compare the simulated diffraction pattern with the experimental data.[22] Since both the initial orientation of the crystallite and the axis of rotation contribute to the final diffraction pattern, the generated diffraction pattern is numerous. Yet after searching all the possible combinations with the assistance of computer, we find that there is only one case that agrees perfectly well with the experimental data. Figure 3e−g demonstrates a group of simulated diffraction patterns, which are almost identical to those illustrated in Figure 3b−d. It is noteworthy that in Figure 3e−g not all the spots elongate radially, which is consistent with the experimental observation. By analyzing the diffraction data we know that [111] of the crystallite at sites 1, 2, and 3 point to the direction (0.12, 0.12, 0.98), (0.45, 0.14, 0.88), and (0.52, 0.096, 0.85), respectively.[23] The orientation of the coordinate system is indicated in Figure 3. By carrying out systematic X-ray diffractions, we conclude that crystallite $A_i$ in Figure 1c initially contacts the substrate roughly with (111). When the crystallite develops, the orientation of the newly grown parts rotates with [110] as axis, which lies on a plane parallel to the substrate and is perpendicular to the direction of branch development. This growth behavior persists, hence the face touching the substrate changes continuously. At site $B_i$, the bottom surface becomes roughly (110) and the advancing direction becomes [100]. From the symmetry of the crystallites in the aggregate branch and the X-ray diffraction presented in Figure 3, we can infer the evolution of the crystallographic orientation over the whole aggregate branch. Suppose during the growth of $B_i$, its rotation axis remains [110], and keeps in the plane parallel to the substrate and is perpendicular to the direction of branch development. As the branch develops further, the bottom face of the crystallite on the tip of the branch changes back to one of the equivalent $(\bar{1}\bar{1}\bar{1})$ and the crystallite turns out to be $A_{i+1}$, a mirror image of $A_i$. This picture is in excellent agreement with the morphological observations of the optical microscopy and atomic force microscopy.

Our previous studies have shown that the crystallites of $NH_4Cl$ grow on the glass substrate by nucleating at the concave corner of the crystallite and the substrate.[17−20] The heterogeneous nucleation at the concave corner acts as the step source. During this nucleation-mediated growth, the substrate is actually inhomogeneous: one edge of the concave corner is the crystal terrace, whereas the other one is the glass substrate. As we presented in a separate paper,[20] once an embryo of nucleus appears at the concave corner, the asymmetric surface tension tends to deform the embryo. So the orientation of the nucleus is slightly rotated. This effect maintains as long as the crystallization is promoted by the nucleation-mediated layered growth. Eventually the crystallographic orientation of each layer deviates. The evidence of the corner-assisted growth has been achieved by atomic force microscopy and is shown in Figure 4, where the whole crystallite of type *B* and parts of a crystallite of type *A* can be identified. It is clear that the steps originate from the concave corner of the crystallite facet and the substrate. Figure 4 supports our previous argument that the crystallization is carried out by layer-by-layer growth, and successive nucleation at the concave corner contributes as the step source.

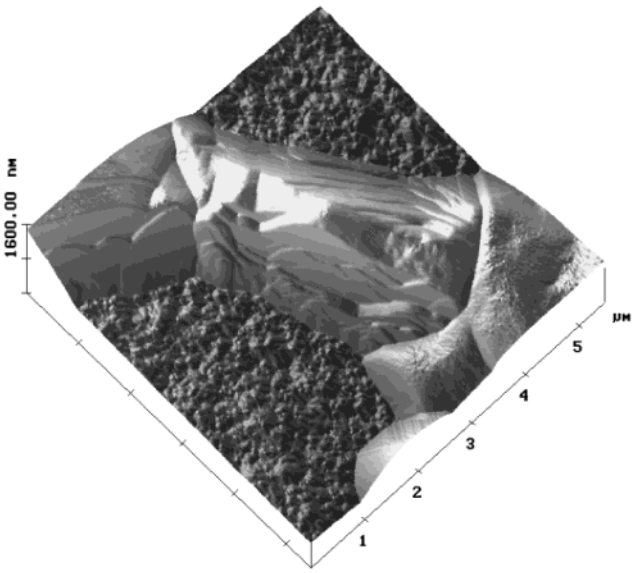


**Figure 4.** AFM view of a crystallite of type *B* in the zigzagged branch. One may find that the steps initiated from the concave corners of the crystallite facet and the substrate.

The theory of periodic bond chain (PBC) has been developed to predict the crystal morphology.[24,25] According to this theory the PBC is defined as a chain with strong bonds, or bonds in the first coordination sphere, between the growth units. Those layers containing two or more PBCs are defined as F faces or flat faces. S face or stepped face is a slice that contains only one PBC; K face or kinked face stands for a slice that does not contain PBC at all. It is known that the point group of $NH_4Cl$ is $P_{m\bar{3}m}$, and $NH_4^+$ and $Cl^-$ are located at (0,0,0) and (1/2,1/2,1/2), respectively. $NH_4Cl$ has strong bonds in $\langle 100\rangle$, $\langle 110\rangle$, and $\langle 111\rangle$. Accordingly the F slices of $NH_4Cl$ are {100}, {110}, and {111}. {100} and {111} faces are nonpolar ones, and {110} face is polar. In a polar solvent, such as water, the polar F slice seems to be suppressed.[19] Therefore {100} and {111} faces are most easily observed in aqueous-solution-grown $NH_4Cl$ crystallites. To illustrate how the crystallographic orientation changes during the growth, we schematically plot the evolution of the crystallographic orientation over a zigzagged branch based on the results of MXRD and PBC theory, as shown in Figure 5. Suppose {100} is the dominant face. At site α of Figure 5, the crystallite contacts the substrate with $(\bar{1}\bar{1}\bar{1})$, with the top face of the crystallite being (111) and the side faces (100), (010), and (001). In addition to {100} and (111), $(11\bar{1})$, $(1\bar{1}1)$, and $(\bar{1}11)$ also exist. Yet according to ref 26, {111} tend to be small since $\langle 111\rangle$ is the fast growing direction.[27] As shown in Figure 5, at site α the crystallite elongates along one of its corners (this situation is similar to that shown in Figure 2a−b, and is decided by the local concentration field). The crystallographic orientation of each grown layer rotates slightly with respect to axis $[1\bar{1}0]$. As indicated in Figure 5, when the growth front reaches site $\beta$, the crystallographic orientation of the newborn layer has rotated for 35° (i.e., from (111)-up to (110)-up). Meanwhile, the two side faces of the elongated crystallite become (100) and (010). The rotation continues as the crystallite grows further. At site α′, $(11\bar{1})$ becomes the top face ($[11\bar{1}]$ is normal to the substrate). Meanwhile the face on the growth front becomes $(00\bar{1})$, which develops much slowly than {111}. Thereafter the fast growth takes place along $[1\bar{1}\bar{1}]$ (or $[\bar{1}1\bar{1}]$)

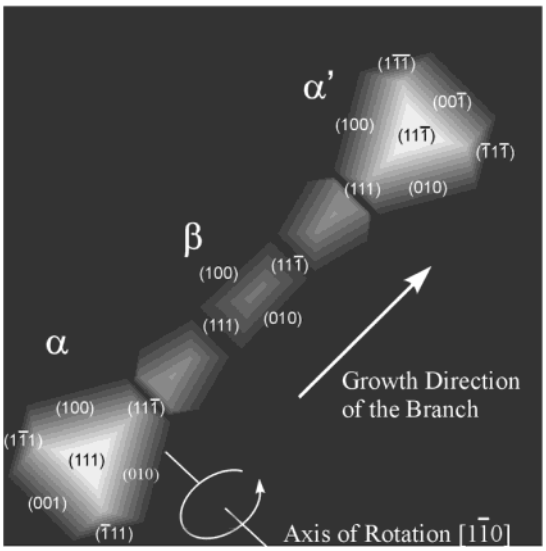


**Figure 5.** Schematic diagram to show how the crystallographic orientation evolves in the branch. The aggregate grows in the direction from α to α′, and the crystallographic orientation rotates continuously with the axis shown in the picture. Note that the polyhedrons in the picture are merely the guide of eyes to illustrate the crystallographic orientation at each site. They are not necessarily connected to the real morphology of the units in the aggregate branch.

(Figure 5). This process corresponds to that shown in Figure 2d−e. It should be emphasized that although several separate polyhedrons are drawn in Figure 5, they are only the guides of the eyes to illustrate how the crystallographic orientation evolves during crystallization.

The above analysis is further supported by in situ observation of the growing process of the zigzagged branch. In the early stage of the sharpening of the tip of crystallite *A* (Figure 2a), the orientation of the growth front is nearly ⟨111⟩ , whereas in Figure 2f, the growth front along the original growth direction becomes ⟨100⟩ . This difference may lead to a clear change of the interfacial growth rate. We trace the growing tip of a zigzagged branch as a function of time. During the elongation of the crystallite tip (process 1 in the insert of Figure 6), the growth rate of the tip first increases and then decreases (as illustrated by curve 1 in Figure 6), which corresponds to the gradual sharpening, and then broadening of the growth front. Before the growth along this direction stops completely, corner sharpening along the other direction (process 2 in Figure 6) starts. Curve 2 in Figure 6 shows that the growth rate increases gradually first, and then decreases. We expect that the deceleration of the interfacial growth is associated with the change of the crystallographic orientation of the growth front from nearly (111) to roughly (100). Before process 2 stops completely, one of the corners of the front-most crystallite starts to grow (process 3 in Figure 6) with an increasing growth rate (curve 3 in Figure 6).

As illustrated by the arrows in Figure 2, the separated crystallites in the zigzagged branch are actually generated by repeated formation of ditches on the branch. Within a crystallite the crystallographic orientation changes continuously, as indicated in Figure 3. As a result, stress is generated in the crystallite. Meanwhile a stress-induced interfacial instability may occur to the crystallite surface.[1,6] It has been reported that a nominally flat surface profile of an elastically stressed solid can rapidly evolve into a cusped surface with smooth tops and deep crack-like grooves by surface diffusion.[7] The characteristic length of the surface pattern can be estimated by $k_{max}$, the upper limit of the linearly unstable wavevector. Similar to conventional

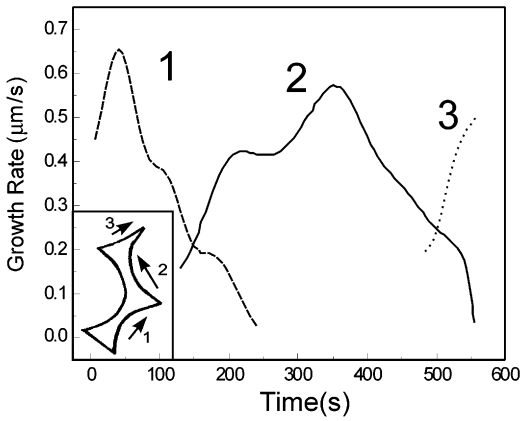


**Figure 6.** The growth rate of the front-most tip measured as a function of time. Curve 1 corresponds to a process as that shown in Figure 2a−e (or, process 1 in the inset). The growth along this direction decelerates gradually. Before it ceases completely, the growth along the other direction starts by sharpening the crystallite corner, as that shown in Figure 2f (or the process 2 in the inset). The growth rate of the front-most tip along this direction is shown by curve 2, which increases first and decreases thereafter. The decreasing of the growth rate in curve 2 again corresponds to the faceting of the growth front. Curve 3 corresponds to the sharpening of the crystallite corner along the other direction (the process 3 in the inset). The change of the growth rate may be due to the change of the crystallographic orientation at the growth front.

Mullins−Sekerka instability,[1,28,29] which takes place at long wavelength and is driven by diffusion, here the instability is induced by stress.[1,9,10] Suppose the crystal is subjected to an uniaxial stress, and the strain is $\epsilon_{xx}$, it follows that the critical unstable wavelength can be expressed as

$$\lambda_0 = \frac{2\pi}{K_{max}} = \frac{\pi\gamma(1-\sigma^2)}{E\epsilon_{xx}^2} \qquad (2)$$

where $E$ is the Young's modulus of the material, $\sigma$ is the Poisson coefficient, and $\gamma$ is the surface tension of growing interface. The strain $\epsilon_{xx}$ is estimated as follows. The elongation of the diffraction spots as that shown in Figure 3 indicates that within each crystallite the crystallographic orientation has been continuously changed for two to three degrees. Taking the length of the crystallite as 30 $\mu$m and the thickness of the crystallite as 2 $\mu$m, it follows that the strain inside the crystallite is of the order of $1.5 \times 10^{-3}$. This value, together with other material parameters of $NH_4Cl$,[30] yields $\lambda_0 = 45$ $\mu$m according to the above equation. This means that when the size of a crystallite reaches $\lambda_0$, its top surface will be unstable and wrinkles may develop to separate the crystallite.[20] The crystallite size will be of the order of $\lambda_0/2$, which is consistent with our experimental observations.

It is noteworthy that even though the crystallite size varies for different driving forces of crystallization, the number of crystallites within each period remains unchanged. Experiments show that crystallite size decreases rapidly by increasing the equivalent driving force of crystallization. Meanwhile, the average growth rate of the aggregate increases, as shown in Figure 7. When the crystallite grows faster, we expect that the rotation of the crystallographic orientation becomes more rapid. This means that the stress will be increased more quickly. Hence the crystallite becomes smaller in size. Indeed this tendency has been experimentally observed, as illustrated in Figure 7. If the driving force for the crystallization becomes so high that nucleation occurs everywhere, then we expect that the regularity among the crystallites will disappear.

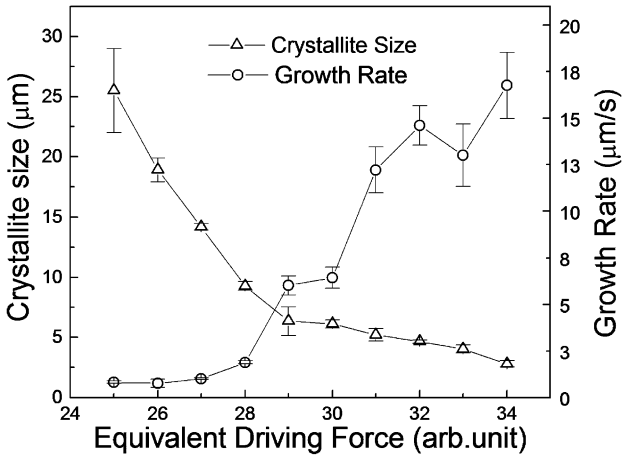


**Figure 7.** The average size of crystallite and the average growth rate of the aggregate branch measured as a function of the equivalent driving force of crystallization. By increasing the driving force, the crystallite size decreases and the branch growth rate increases. In our experiment the driving force is controlled by evaporating water in the agarose gel. The evaporation rate is adjusted by the flow of dried nitrogen gas. The driving force increases when the nitrogen flux is high. In this figure we use the nitrogen flux flowing through the growth cell to represent the driving force of crystallization.

The role of nucleation on growth pattern has been studied before. Some concepts, such as nucleation-limited aggregation,[31] heterogeneous 2D nucleation-induced instability,[32] and self-epitaxial nucleation[33] have been proposed. However,concerning the formation of zigzag branch, previous studies are still not satisfactory in explaining why the structural matching prescriptions of the octahedral and hexahedral modifications should be different. Or more specifically, why in the aggregate the hexahedral modification occurs via $(211) \leftrightarrow (\bar{2}\bar{1}\bar{1})$, whereas the octahedral modification takes place via $(01\bar{1}) \leftrightarrow (102)$.[17,19] The experimental observations presented in this article provide unambiguous evidence that the zigzagged branch is, as a matter of fact, generated by the consecutive rotation of crystallographic orientations, which eventually contributes to the long-range morphological and orientational orders in the aggregate. It is indicated clearly that both the axis of rotation and the crystallographic faces contacting the substrate decide the final morphology of the aggregate. If a crystallite initially contacts the substrate with its {001} face and rotates with [110] as axis, periodic roughening transitions as that reported in ref 20 appears. If, however, the crystallite initially contacts the substrate with (111), and rotates with $\langle 110 \rangle$ as the axis, a regularly zigzagged branch developing along $\langle 1\bar{1}0 \rangle$ as we report in this article will be observed.

## IV. Conclusion

In this article the long-range correlation of the crystallographic orientations in aggregating crystallites of $NH_4Cl$ has been studied by analyzing the data of micro-X-ray-diffraction, atomic force microscopy, and in situ interfacial growth processes. The experiments indicate that there exists a consecutive rotation of crystallographic orientation in each crystallite, which may be responsible for the morphological regularity of the aggregate branches. The continuous change of the crystallographic orientation in crystallization may root from the deformation of the embryo of the nucleus by inhomogeneous surface/interface tensions. We suggest that the phenomena reported here have general interest for the nucleation-mediated growth and would help to understand the long-range ordering effect in aggregating crystallites.

**Acknowledgment.** This work was supported by the grants from the Ministry of Science and Technology of China (No. G1998061410) and the National Science Foundation of China (Nos. 19974014 and 10021001). Authors thank the Station of X-ray Topography on the beam line 4W1A of BSRF for help, and Dr. M. Plapp and Dr. V. Fleury for discussions.

## References and Notes

(1) Pimpinelli, A.; Villain, J. *Physics of Crystal Growth*; Cambridge University Press: Cambridge, 1998.

(2) Murry, C. B.; Kagan, C. R.; Bawendi, M. G. *Science* **1995,** *270*, 1335.

(3) V. A. Shchukin et al., *Phys. Rev. Lett.* **1995,** *75*, 2968.

(4) Tersoff, J.;, Teichert, C.; Lagally, M. G. *Phys. Rev. Lett.* **1996,** *76*, 1675 and references therein.

(5) Eaglesham, D. J.; Cerullo, M. *Phys. Rev. Lett.* **1990,** *64*, 1943.

(6) Politi, P.; et al. *Phys. Rep.* **2000**, *324*, 271 and references therein.

(7) Berrehar, J.; et al. *Phys. Rev. B* **1992,** *46*, 13487.

(8) Müller, J. Ph. D thesis, McGill University, Montreal, 1998.

(9) Asaro, R. J.; Tiller, W. A. *Metall. Trans.* **1972,** *3*, 1789.

(10) Grinfeld, M. A. *Sov. Phys. Dokl.* **1986,** *31*, 831.

(11) Keith, H. D.; Padden, F. J., Jr. *J. Appl. Phys.* **1963,** *34*, 2409.

(12) Singfield, K. L.; Hobbs, J. K.; Keller, A. *J. Cryst. Growth* **1998,** *183*, 683.

(13) Hutter, J. L.; Bechhoefer, J. *J. Cryst. Growth* **2000,** *217*, 332.

(14) Bisault, J.; Ryschenkow, G.; Faivre, G. *J. Cryst. Growth* **1988,** *87*, 221.

(15) Matsuno, T.; Koishi, M. *J. Cryst. Growth* **1989,** *94*, 798.

(16) Tracy, S. L.; Francois, C. J. P.; Jennings, H. M. *J. Cryst. Growth* **1998,** *193*, 374.

(17) Wang, M.; et al. *Phys. Rev. Lett.* **1998,** *80*, 3089.

(18) Liu, X. Y.; et al. *J. Cryst. Growth* **2000,** *208*, 687.

(19) Strom, C. S.; Liu, X. Y.; Wang, M. *J. Phys. Chem. B* **2000,** *104*, 9638.

(20) Li, D. W.; Wang, M. To be published.

(21) Klug, H.; Alexandev, L. *X-ray Diffraction Procedures for poly Crystalline and Amorphous Matevials*, 2nd ed.; Wiley: New York, 1974.

(22) Before carrying out computer simulation, we first determine the coordinates of the center of each elongated diffraction spot in the experimental diffraction pattern. The orientation of a crystallite is characterized by Euler angles $\theta$, $\varphi$, and $\psi$. In calculation the wavelength of X-ray is set between 0.7 and 2.2 Å. $\theta$, $\varphi$ and $\psi$ are changed with a step of 2 mRod. This step size corresponds to a linear separation of about 50 microns in the diffraction spectrum in our experiment. At each step the diffraction pattern is calculated and compared with the experimental data. Once a best-fit combination of $\theta$, $\varphi$, and $\psi$ is found, we continue to determine the axis of the orientation rotation and the degree that the crystallite has been rotated in a similar way. If the computed direction of the spot elongation is in agreement with the experimental observation, we conclude that the correct axis of rotation has been found. It is noteworthy that the noise-to-signal ratio in our experiments is not high, so many high-indexed diffraction spots cannot be identified. As a matter of fact, the analysis of the diffraction spots on the image plate shows that the diffraction coming from $hkl > 2$ is so weak that those spots are virtually not seen. For this reason we only consider $hkl \leq 2$in the computer calculation.

(23) Here we use (cos α, cos $\beta$, cos $\gamma$) to characterize the normal of (111), $\vec{n}$ , with respect to the axes $\vec{x}$, $\vec{y}$, and $\vec{z}$, where, α, $\beta$, and $\gamma$ are the angles between $\vec{n}$ and $\vec{x}$, $\vec{y}$, $\vec{z}$, respectively.

(24) Hartman, P. *Acta Crystallogr.* **1958,** *11*, 365.

(25) Bennema, P. In *Handbook of Crystal Growth*; Hurle, D. T. J., Ed.; Elsevier: New York, 1993; Vol. 1a.

(26) Chan, S. K.; Reimer, H.-H.; Kahlweit, M. *J. Cryst. Growth* **1976,** *32*, 303.

(27) When the supersaturation is higher than 0.2, it has been found $\langle 111 \rangle$ is the fast growth direction. See ref 26 for details.

(28) Ming, N.-B. *Fundamentals of Crystal Growth Physics*; Shanghai Science and Technology, Shanghai, 1982; Chapter 8.

(29) Chernov, A. A.; *Modern Crystallography III: Crystal Growth*, Springer-Verlag: Berlin, 1984.

(30) Winkler, B.; et al. *J. Phys.: Condens. Matter* **2000,** *12*, 2093.

(31) Ming, N.-B.; Wang, M. Peng, R.-W. *Phys. Rev. E* **1993,** *48*, 621.

(32) Liu, X. Y. *J. Cryst. Growth* **2002,** *237−239*, 101.

(33) Liu, X. Y. *J. Cryst. Growth* **2002,** *237−239*, 106.